Distribution and properties of magnetic flux ropes in Titan's ionosphere

C. J. Martin[1], C. S. Arridge[1], S. V. Badman[1], C. T. Russell[2], H. Wei[2]

[1]Physics Department, Lancaster University, Bailrigg, Lancaster, LA1 4YB, United Kingdom.
[2]Department of Earth, Planetary and Space Physics, University of California, Los Angeles, CA, USA.

Key Points:

- 85 flux ropes are detected in Titan's ionosphere using all of Cassini's flybys of Titan
- Flux ropes are present when Titan is in dynamic areas of Saturn's magnetosphere
- Fitting a force free flux rope model leads to the conclusion that on average they are unlikely to be force free

Corresponding author: C. J. Martin, carleymartin@hotmail.com

Abstract

Titan's magnetic environment is a dynamic and unique place. We detect 85 flux ropes during all the Cassini flybys of Titan from 2005-2017. Analysis describing the location of flux ropes in Titan's ionosphere as well as where Titan is in Saturn's magnetosphere shows that the flux ropes are more often found when Titan is in the noon sector of Saturn's magnetosphere. A secondary peak of occurrence is found in the post midnight area, where it is expected that Saturn's magnetosphere is highly dynamic. We also find that the flux rope occurrence is correlated with the average electron density profile of Titan's ionosphere. A force-free model is utilised to estimate the radii and core magnetic field strength of the flux ropes. We find a large range of radii from 150-500 km with a small number of very large flux ropes (500-1000 km) and a range of core field strengths of 1-15 nT, again with some much larger values (20-40 nT). The model also shows that more flux ropes are right-handed than left-handed in twist, however we are unable to determine if there is a physical reason or if this is due to an observer bias. Additionally, we evaluate the goodness of fit for the model in each instance and conclude that, on average, the flux ropes may be better represented by a non-force-free model.

1 Introduction

Flux ropes are bundles of magnetic flux that are twisted around a central axial core magnetic field with an increasingly tangential field with radial distance from the centre. Flux ropes are ubiquitous in plasma regimes across the solar system and have been found in the ionospheres of the terrestrial planets: Venus and Mars (e.g., Russell & Elphic, 1979; Vignes et al., 2004), in the magnetosphere of Mercury (e.g., Slavin et al., 2010), on the solar surface (e.g., Mouschovias & Poland, 1978) and in the solar wind where they are named magnetic clouds (e.g., Burlaga et al., 1982). Flux ropes are the results of a highly dynamic and interactive magnetic and plasma environment. Flux ropes on the solar surface are thought to be a precursor to coronal mass ejections and solar flares (Chen & Shibata, 2000), and as such flux ropes could be a useful diagnostic tool to uncover the various dynamics of the ionospheres of the terrestrial planets and giant planet moons.

The location of flux ropes around a planetary body can infer their source mechanism, i.e. production at Earth's magnetopause would elicit a conclusion that the solar wind and reconnection are a source mechanism for flux transfer events at Earth (Russell et al., 1985). Similarly, flux ropes in the magnetotail current sheet show that a possible source can be found in tail reconnection (Slavin et al., 2003). Flux ropes at Venus have been theorised to have a number of generation mechanisms, most of which would show a locational bias in detection. For example, if flux ropes were generated by the Kelvin-Helmholtz instability at the ionopause (Wolff et al., 1980) then we might expect an occurence bias close to the ionopause with properties of flux ropes changing with distance from the ionopause. If they were generated by gravity waves and dynamo action in the ionosphere (Luhmann & Elphic, 1985) then we might expect an occurence bias close to the "nose" of the induced magnetosphere. In contrast, flux ropes produced by random magnetohydrodynamic flows in the ionosphere (Kleeorin et al., 1994) might not show any bias.

Flux ropes in Titan's ionosphere were first examined by Wei, Russell, Zhang, and Dougherty (2010), where the authors found two unusually large spikes in the magnetic field magnitude in Cassini magnetometer data. The authors compared the magnetic signatures to a force-free flux rope model (e.g., Burlaga, 1988) and concluded that they were flux ropes. Additionally, Wei, Russell, Zhang, and Dougherty (2010) compared Titan's flux ropes to matured flux ropes in Venus' ionosphere. During the T42 flyby, a very pronounced peak in magnetic field magnitude was discovered by Wei et al. (2011) which exceeded all known magnetic field values previously seen at Titan. The authors show that the structure is likely a flux rope, and discuss the possibility of the rope originating from

the interaction of Titan with solar wind plasma when Saturn's magnetopause is pushed back inside Titan's orbit.

Titan is in mildly eccentric orbit around Saturn with a semi-major axis of 1.22×10^6 km (20.27 R_S, where 1 R_S = 60268 km) and an eccentricity of ($\varepsilon = 0.0288$) which gives Titan a 1.17 R_S difference in distance from Saturn between perikrone and apokrone. It's orbit is almost in Saturn's equatorial plane with an inclination of 0.3485 degrees. The sub-solar position of Saturn's magnetopause is often found at a bimodal distribution of positions (21 and 27 R_S (Pilkington et al., 2015)). During times of high solar wind dynamic pressure, it is common to find the magnetopause inwards of 20 R_S and hence Titan is often found within Saturn's magnetosheath and even, on rarer occasions, in the solar wind itself (Bertucci et al., 2015). However, in general, Titan resides inside the magnetosphere of Saturn where the equatorial region is a varied and dynamic place compared to the solar wind.

Saturn's equatorial current sheet (e.g., C. Arridge, Russell, et al., 2008) is found in all local time sectors unless high solar wind dynamic pressure contracts the magnetosphere and the current sheet is no longer present in the day side (C. Arridge, Russell, et al., 2008). Additionally, the current sheet has a number of movements that cause the current sheet to be offset from the equator near which Titan lies. The seasonal bowl shape (C. Arridge, Khurana, et al., 2008) causes the whole current sheet to move off the equator increasingly with radial distance due to the solar wind dynamic pressure and the current sheet mass. Superposed are periodic flapping movements (C. Arridge et al., 2011; Provan et al., 2012), which cause the current sheet to flap at the near the rotation rate of the planet, and aperiodic random waves that cause large disturbances to the current sheet (Martin & Arridge, 2017, 2019). Together these processes act to form a highly dynamic environment in which Titan resides (Simon et al., 2010, 2013; Achilleos et al., 2014).

Titan's ionosphere itself is mainly formed through magnetospheric electron impacts and solar radiation (e.g., Cravens et al., 2005; Agren et al., 2007), from the thick and extended atmosphere. Titan's low gravity and dense atmosphere means that the atmosphere is extended to over 1000 km in altitude (Yelle et al., 2006), and as such the peak ionospheric electron density is found at altitudes between 1100 - 1200 km (Keller et al., 1992). As Titan has no measurable intrinsic magnetic field (Wei, Russell, Dougherty, et al., 2010), the interaction between the moon and Saturn's magnetic field is that of an induced draped magnetosphere where Titan's extended ionosphere 'captures' the rotating magnetic field of Saturn to form a draped magnetic field with defined tail and current sheet (Ness et al., 1982). Similar in form to the draping of the interplanetary magnetic field around Venus.

The same draping process occurs when Titan is in the magnetosheath or solar wind, however the draped field is now sourced from the IMF. Titan is also expected to form a well-defined bow shock when present in the solar wind (Bertucci et al., 2015; Feyerabend et al., 2016; Omidi et al., 2017). Titan's interaction with Saturn's magnetopause can also give rise to another magnetic phenomena at Titan - fossil fields (Neubauer et al., 2006; Bertucci et al., 2008). Fossil fields are remnants of magnetic field deposited in Titan's ionosphere when the magnetic field in a different magnetic environment was draped around Titan (i.e., solar wind plasma and magnetic field can be found in Titan's ionosphere when Titan is inside of Saturn's magnetopause as it was deposited there during a recent excursion into the magnetosheath.) Bertucci et al. (2008) estimates that the lifetime of fossil fields are on the order of 3 hours. Wei et al. (2011) discussed the possibility of flux ropes originating, like fossil fields, from a different magnetic environment from the current one, where possible solar wind plasma was found inside the flux rope surrounded by magnetospheric plasma.

In this paper, we use the entire Cassini magnetometer data set to survey the Titan flybys for flux ropes to contribute to our understanding of Titan's unique induced

magnetosphere. This study presents a location analysis of the 85 flux ropes at Titan, with emphasis on where on Titan the flux ropes are found along with where Titan is located in Saturn's magnetosphere. A force-free model is adapted to fit the magnetic field signatures where radii, axial magnetic field, handedness, and flux content of the flux ropes is explored along with the restrictions and assumptions of the model used. Finally, a discussion of the flux ropes will conclude with a comparison with flux ropes at Mars and Venus.

2 Methods

Cassini magnetometer data (Dougherty et al., 2004), with a resolution of 1 second, is utilised to detect peaks in magnetic field magnitude along each of the 127 Titan flybys. Elphic and Russell (1983b, 1983a) stated that a flux rope is a discrete individual excursion of magnetic field where a peak in magnetic field magnitude is larger than the surrounding magnetic field. Within this study we define a 'larger magnitude' as > 1 nT due to the average background field being on the order of 1-5 nT and fluctuations within the background unrelated to flux ropes or environment are < 0.5 nT. Hence, we plot magnetic field magnitude with altitude to determine if a flux rope is present. An example of an altitude plots with a single flux rope on the inbound flybys of T30 is shown in Figure 1 along with an example of a flyby with two flux ropes on the inbound of T84. Cassini flybys of Titan are named T(*number of letter corresponding to flyby*) where TA is the first flyby and T3 is the first flyby after the release of the Huygen probe.

We then verify that the magnetic field fits a flux rope signature using minimum variance analysis (Sonnerup & Cahill Jr, 1967) (MVA) on the smaller time series between the initial increase in magnetic field magnitude to when it reaches the background level again. In the ideal case, MVA allows us to determine the directions of maximum, intermediate and minimum variance. At Mercury it was found that maximum variance direction was tangential to the flux rope, the intermediate direction was along the flux rope axis, and the minimum variance direction was in the radial direction (in cylindrical co-ordinates). However, in this study we found that at Titan the maximum variance direction was along the axial direction, thus the intermediate and minimum variance directions could be combined to give the tangential direction, assuming the radial field is zero.

The variance directions are identified as eigenvectors with associated eigenvalues λ_1, λ_2 and λ_3 for maximum, intermediate and minimum directions respectively. Ratios of these eigenvalues allow us to infer the ability of the variance analysis to find a distinct co-ordinate system, where the ratio, $\frac{\lambda_1}{\lambda_2}$, gives the degeneracy of the eigenvectors. As we are constructing a co-ordinate system, we require each eigenvector to be distinct and non-degenerate and as such the eigenvalues are required to be distinct, and the ratio gives a measure of this. We accept eigenvalue ratios of two or more for both ratios, however most magnetic field time series in this study give eigenvalue ratios of 10 or more, i.e. the variance directions are distinct and non-degenerate. For comparison, studies at other planetary bodies use an eigenvalue limits of five (Smith et al., 2017) and eight (Briggs et al., 2011) however, some believe that changes in the acceptance limit does not strongly effect the results (e.g., DiBraccio et al., 2015).

The handedness of the flux rope corresponds to the direction of which the tangential field curves around the axial field. If a flux rope is right handed and the axial field is along z then the tangential field is anti-clockwise around z. Conversely, a left handed flux rope has a clockwise tangential field.

3 Spatial Distribution of Flux Ropes

At Titan, we find that the flux ropes are detected in the ionosphere. Figure 2 shows that the highest occurrence rate of flux ropes is around 1050-1100 km which is near the

estimated peak of the electron density (e.g., Keller et al., 1992; Edberg et al., 2010; Ågren et al., 2009) and decreases either side. We also note that due to Cassini's closest approach to Titan being above 900 km, we cannot show a lower limit for their detection as they may occur lower than Cassini has probed, and as such the decrease in occurrence near 900 km is assumed to be due to an observer bias.

As described earlier, we know that Titan is exposed to a number of different magnetic and plasma regimes as it travels along its orbit. In the noon sector, Titan is likely to interact with the magnetopause, in the tail and flanks Titan is exposed to the current sheet dynamics which can see Titan in either lobe of Saturn's magnetic field or within the current sheet (Simon et al., 2010). Figure 3 shows the occurrence rate of flux ropes normalised to the number of flybys in each local time sector which sample below 2000km (taken from figure 2) of 1 hour SLT (Saturn Local Time) width. The vast majority of flux ropes occur in the dayside of Saturn with a smaller number in the 23-3 SLT sector. The events that make up the 15-20 SLT sector total five events which occur when Titan is within Saturn's magnetospheric current sheet.

The axial direction for each flux rope, as determined from MVA, allows us to infer the orientation of the flux rope compared to the surface of Titan, where 90° is parallel to the surface of Titan and 0/180° is perpendicular. We are only interested in determining if the flux rope is parallel or perpendicular to the surface of Titan, hence orientations of 180° - 360° are folded into the 0° - 180° parameter space. We find a large spread of orientations with a maximum occurrence around 90° and minima at 0° and 180°. This demonstrates that the flux ropes are found in the plane of the expected draped field around Titan, e.g. tangential to the surface. Figure 4 shows this orientation bias.

The Titan-Ionosphere-Interaction-System (TIIS) is an orthogonal coordinate system centred at the centre of Titan where $\hat{y}$ is positive along the Titan-Saturn line, $\hat{x}$ is along the expected corotation direction, and $\hat{z}$ completes the right handed system. In the TIIS coordinate system, we can find the position of the flybys with respect to the expected corotation direction. Figure 5 shows a depression in occurrence where the tail of Titan's induced magnetosphere is expected if assuming Saturn's magnetospheric plasma population and magnetic field are strictly corotating, i.e., the paucity of flux ropes in figure 5a, between $0 < Y_{TIIS} < 1$, $-1 < X_{TIIS} < 0.5$). This assumption is as accurate as possible for the majority of Titan flybys as there are no in-situ measurements of the velocity and direction of Saturn's magnetospheric plasma whilst Cassini is in Titan's ionosphere, and the rate of change from when Cassini is sampling Saturn's magnetosphere to the sampling of the flux ropes is large and the environment is dynamic in that time frame.

4 Force-free Modeling

Force-free assumes that the $\mathbf{j} \times \mathbf{B}$ force density in the flux rope is equal to zero. Hence, the assumption is that the currents present in the flux rope are negligible or field aligned, and the magnetic pressure force $\left(\frac{B^2}{2\mu_0}\right)$ is balanced with the magnetic tension force $\left(\frac{B^2}{2\mu_0 R_c}\right)$ where B is the magnetic field magnitude, μ_0 is the permeability of free space and R_c is the radius of curvature of the magnetic field. A number of authors have discussed how a force-free flux rope might represent a flux rope in equilibrium, in its lowest energy state (Osherovich et al., 1995). As such, a developing or evolving flux rope would not appear to be force free and the fit of a force-free model to a flux rope would depend on the "maturity" of the flux rope Wei, Russell, Zhang, and Dougherty (2010).

Minimum variance analysis, described earlier, is used to rotate the magnetic field into a flux rope coordinate system where at Titan we find that the maximum variance

direction in Cartesian coordinates gives the axial field direction. The final magnetic field component (radial) is assumed to be a constant zero in the force-free assumptions. The three magnetic field components are modeled from Ampere's Law in cylindrical coordinates to give:

$$B_A = B_0 J_0(\alpha R) + b_0, \tag{1}$$

$$B_T = H B_0 J_1(\alpha R), \tag{2}$$

$$B_R = 0, \tag{3}$$

where B_0 is the core axial magnetic field, J_0 and J_1 are the zeroth and first order Bessel functions, b_0 is a magnetic offset in the axial direction. α is a constant of 2.4048 representing the first root of the zeroth order Bessel function. H is the handedness of the flux rope and can take values 1 or -1.

R is radial distance from the flux rope centre during the fly-through, we do not directly know R yet and as such we use a proxy, u. u ranges from -1 at the inbound edge of the flux rope, to +1 at the outbound edge. Equation 4 can be used to estimate αR:

$$\alpha R = \alpha \left(\sqrt{\left(\frac{Y_0}{R_0}\right)^2 + u^2 \left(1 - \left(\frac{Y_0}{R_0}\right)^2\right)} \right), \tag{4}$$

where Y_0 is the closest approach distance to the centre of the flux rope, R_0 is the radius of the flux rope. Hence $\left(\frac{Y_0}{R_0}\right)$ is the impact factor, or ratio of closest approach to radius which will equal unity at the flux rope edge and zero directly at the centre (Lepping et al., 2017). The actual radius can be calculated knowing the trajectory, velocity, and position of the spacecraft relative to the flux rope. We assume at Titan that the flux ropes are stationary. With this approximation, the radius is found using the following equation derived from the geometry of the flux rope encounter:

$$R_0 = \frac{V t \sin(\phi)}{2 \sin\left(\cos^{-1}\left(\frac{Y_0}{R_0}\right)\right)}, \tag{5}$$

where V is the spacecraft velocity, t is the time in seconds since entry to the flux rope, ϕ is the angle between the flux rope axis and the trajectory.

Furthermore, one can calculate the flux content, Φ, of the flux rope using the following equation:

$$\Phi = \frac{2\pi}{\alpha} B_0 R_0^2 J_1(\alpha) \tag{6}$$

The model, consisting of four free parameters B_0, Y_0/R_0 (impact factor), b_0 and H, is fitted to the magnetometer data using non-linear least squares, minimising the reduced χ^2 using the Levenberg-Marquardt algorithm. With the restriction that H can only take the values 1 and -1. This restriction is imposed by fitting the model twice, once for either handedness, and selecting the lowest χ^2 value. Uncertainties are estimated using the covariance matrix formed during the final iteration of fitting which is calculated using the Jacobian matrix. The square root of the diagonal elements of the covariance matrix give the standard deviation of each fitted value, and hence a measure of uncertainty in each parameter. The off-diagonal elements give a measure of the covariance between each of the fitted parameters, and non-zero values of off-diagonal elements show the variables to be fitted are dependant on each other.

An example of a force-free model fitted to magnetometer data is found in Figure 6 for a flux rope on T5 in 2005. 49 of the total 85 flux ropes could be fitted using the force-free model to a satisfactory degree (χ^2_ν equal to or below 5 and χ^2 P-value of 0.05 or more). This restriction was to allow the fitting to attempt to fit flux ropes that may

not completely fit the force-free assumptions. The P-value is a probability that, under a null hypothesis (in this case the null hypothesis is that the fitting is no better than a straight line) the χ^2_ν will be greater than the value of χ^2_ν calculated from the data, a value of 0.05 or 5% is a generally accepted significance level. Values of χ^2_ν and χ^2 P-value for each flux rope can be found in supporting information S1.

Figure 7 shows the results of the 49 flux ropes that were fitted to a satisfactory degree, showing the maximum core field strength in a), the flux rope radii in b) and the flux content calculated from these values in c). The binning of the data is unequal to emphasis the spread without a number of null bins, field strength is binned into 1 nT bins from 0-10 nT, then 2 nT bins from 2-40 nT. Radii of the flux ropes is binned as 50 km for 0-500 km and 100 km for 500-1500 km. Flux content is binned as 5 Wb from 0-20 Wb, 20 Wb from 20-200 Wb and 100 Wb from 200-400 Wb.

The main results show that in each parameter of interest there are is a large spread where the maximum field strength ranges from 1-15 nT, the radii from 50-500 km and the flux content from 5 Wb with a long tail up to 400 Wb. The spread of data is large and as such an average value will not be quoted as it is not instructive, however, it is noted that the distributions appear to maximise at lower values and have a large tail. This shows that smaller and weaker flux ropes are more common but large and strong flux ropes are also found at a lower occurrence rate. Additionally, the handedness of the ropes is investigated and it is found that 37 are right-handed and 12 are left-handed. Russell (1990) showed that the handedness of flux ropes at Venus corresponded to the location of the flux rope source. If the flux rope formed on the dusk flank of Venus (note that Venus exhibits retrograde rotation) then these flux ropes were more likely to be left-handed, and a right-handed preference is found on the dawn flank. However, there appears to be no statistical significance to the position or orientation of either handedness at Titan (not shown).

5 Discussion

Titan's environment is highly changeable in that the moon can find itself moving between different magnetic and plasma regimes in short time frames. Titan being present in the solar wind and magnetosheath is controlled by both the magnetopause position and hence solar wind dynamic pressure, and where Titan is along its orbit. Figure 3 shows that when normalised to the number of flybys present in each one hr local time bin, the majority of flux ropes are found between 9-14 SLT with a large peak at 12-13 SLT. We thus conclude that the highly dynamic magnetic environment of the dayside magnetosphere, near the magnetopause, may be a source of initiation of flux ropes, this is displayed in Figure 8 which shows the number of flux ropes found in each SLT sector for each magnetospheric environment.

Additionally, Figure 9 shows the occurrence of flux ropes found in each magnetospheric environment. The red bars show the relative occurrence, relative to the occurrence rate of all flux ropes in each environment. We find that a much higher relative occurrence rate is found when Titan is in the magnetosheath or solar wind. The environment classification is found using Simon et al. (2010, 2013); Kabanovic et al. (2017).

A secondary peak in occurrence is found when Titan is in the post-midnight sector (1-3 SLT). This is presumably driven by a general disturbed environment, related to activity in the magnetotail driven by magnetic reconnection (Vasyliunas, 1983) and where we note that the observed (Arridge et al., 2016) and statistical reconnection X-line from plasmoids/dipolarisations (e.g., Thomsen et al., 2013; Smith et al., 2016, 2018) is close to Titan's orbit.

The final peak in occurrence, between 16-19 SLT, consists of five flux ropes that occur only when the moon is inside the equatorial current sheet, shown in figure 8. Ad-

ditionally, all local time sectors are sampled except 7-8 SLT, however most notable is that flybys with no flux ropes detected are all found within Saturn's magnetosphere and have very few environment changes as defined by Simon et al. (2010, 2013); Kabanovic et al. (2017) compared to encounters with one or more flux ropes. These non-detection flybys are all during times when Titan mainly resides inside either magnetospheric lobe of Saturn (a table of number of flux ropes and environmental changes can be found in the supporting information).

We also discuss the altitude distribution of flux ropes when normalised by the number of hours Cassini spent in each altitude bin. We find that the peak in occurrence is around 1100-1150 km above Titan's surface, which is colocated with the expected electron density peak. There is a large spread in occurrence where the sharp fall at 800-900 km may be an artefact of the Cassini closest approach distances, and that Cassini never goes below 800 km and as such we cannot give a lower estimate on flux rate occurrence height. Hence, we can conclude that the flux ropes are occurring where electron density peaks and their occurrence reduces in correlation with electron density in the ionosphere above 1100 km.

The orientation of the flux ropes, with respect to the surface normal of Titan, is explored in figure 4, where a broad but pronounced peak in orientation is found around 90°. This means that the flux ropes are lying parallel to the surface of Titan, in the plane of the expected draped magnetic field. Implying that the mechanism for production is possibly the interaction of the draped magnetic field and the external environment.

A total of 49 flux ropes fitted the force-free flux rope model to a satisfactory degree (MSE equal to 0.5 or below, χ^2 probability of 5% or less). The main results show that the flux ropes have a large range of core magnetic field values and radii leading to a large range of flux content. As the spread of data is very large, quoting average values for the flux ropes at Titan would be misleading. However, they have a range of magnetic field strength from 1-15 nT and radii of 50-500 km. Figure 10 shows the radius and magnetic field information on a positional plot. The figure shows that there is little dependence on position for radius and magnetic field strength for the flux ropes that were fitted. Non-fitted examples are shown in grey, indicating there is no positional dependence of the effectiveness of fitting a force-free model. Therefore, we conclude that the position of the flux ropes at Titan is not an effective indicator of which mechanisms may be inducing their formation.

The closest comparison of ionospheric flux ropes may be found in Venus' ionosphere, where flux ropes are frequently observed. The flux ropes here are generally on the order of 10s km in size and varied field strengths inside the flux ropes that range from 1-100 nT (e.g., Elphic et al., 1981; Elphic & Russell, 1983b; Luhmann & Elphic, 1985; Kleeorin et al., 1994; Ledvina et al., 2002; Wei, Russell, Zhang, & Dougherty, 2010). Zhang et al. (2012) shows a secondary population of giant flux ropes on the order of 100s km in size and a flux content of 1000s Wb. In comparison, the flux ropes at Titan have similar spatial scales to the larger population described by Zhang et al. (2012), however have much lower magnetic field strength values on average, attributed to the lower surrounding magnetic field strength.

At all points of this study, we have attempted to reduced the bias produced by Cassini's trajectory, however as described earlier when discussing the altitude occurrence, it is sometimes difficult to remove all biases due to position of Cassini in TIIS coordinates or the changing value of closest approach to the moon. As described, Cassini encounters Titan in every local time hour except 7-8 SLT, however each encounter has a different altitude profile and only shows one *slice* through Titan's ionosphere. Hence it is cautioned that averaging values from all flybys is not an accurate representation of the whole system and as such we have shown a large range of variables for flux rope at Titan.

Improvements to modelling flux ropes, and the different models that can be fitted are explored in a companion paper (Martin et al., Submitted) where elliptical cross sections and bent flux ropes are also explored to aid the fitting of the force-free model and ultimately understand the spacial and temporal evolution of flux ropes. The force-free model describes a flux rope at equilibrium, we hence conclude that the force-free model shows a mature and stable flux rope. Other models, such as the non-force free Hidalgo et al. (2002) model, may be able to more accurately describe a developing and changing flux rope with time and hence why we see a reduced number of flux ropes at Titan being adequately fitted by a force-free model.

6 Summary

85 flux rope signatures are detected in Cassini magnetometer data during all 126 flybys of Titan, where numerous flybys have multiple flux ropes along Cassini's trajectory. We discuss the position of Titan in Saturn's magnetosphere and find that, when normalised to the number of flybys in each local time sector, a higher occurrence is present in the noon (9-15 SLT) sector where according to the classification criteria of Simon et al. (2010), Titan experienced both current sheet and magnetosheath magnetic field. Fluctuations between magnetic field regimes can occur over timescales of less than a few minutes and can last indefinitely depending on the location of Titan and Cassini. Additionally, we find that a secondary occurrence peak is present in the post-midnight area where it it is expected to be a turbulent and dynamic magnetic field regime. Additionally, the flybys found with no flux ropes are found only when the magnetic field is lobe-like or has very few regime changes - i.e. enters the current sheet.

The position of the flux ropes with respect to Titan's surface show a correlation with electron density, and large trajectory and sampling biases. Additionally, the orientation is explored using MVA and found that the flux ropes lie parallel to the Titan's surface, implying that the ropes are initiated by the interaction of draped field with surrounding magnetic field, or alternatively have a similar source to fossil fields.

A force-free flux rope model is examined and fitted to the magnetometer data where the model shows a large range of flux rope radii and central magnetic field strengths of the orders of 50-500 km and 1-15 nT respectively. There appears to be no spatial correlation with handedness, size or field strength however this may be a result of a lack of data. We showed that a large number of flux ropes were unable to be fitted with the force-free flux rope model and additional studies of non-force-free models and changes to the force-free model will be examined in the companion paper Martin et al. (Submitted).

Acknowledgments

CJM was funded by a Faculty of Science and Technology studentship from Lancaster University. CSA was funded by a Royal Society Research Fellowship. CJM, CSA and SVB were funded by STFC grant number ST/R000816/1. Cassini MAG data used in this study may be obtained from the Planetary Data System (http://pds.nasa.gov/).

References

Achilleos, N., Arridge, C., Bertucci, C., Guio, P., Romanelli, N., & Sergis, N. (2014). A combined model of pressure variations in titan's plasma environment. *Geophysical Research Letters*, *41*(24), 8730–8735. doi: 10.1002/2014GL061747

Ågren, K., Wahlund, J.-E., Garnier, P., Modolo, R., Cui, J., Galand, M., & Müller-Wodarg, I. (2009). On the ionospheric structure of titan. *Planetary and Space Science*, *57*(14-15), 1821–1827. doi: 10.1016/j.pss.2009.04.012

Agren, K., Wahlund, J.-E., Modolo, R., Lummerzheim, D., Galand, M., Müller-

Wodarg, I., ... others (2007). On magnetospheric electron impact ionisation and dynamics in titan's ram-side and polar ionosphere-a cassini case study. *Annales Geophysicae*, *25*, 2359–2369. doi: 10.5194/angeo-25-2359-2007

Arridge, Eastwood, J. P., Jackman, C. M., Poh, G.-K., Slavin, J. A., Thomsen, M. F., ... others (2016). Cassini in situ observations of long-duration magnetic reconnection in saturns magnetotail. *Nature Physics*, *12*(3), 268. doi: 10.1038/nphys3565

Arridge, C., André, N., Khurana, K., Russell, C., Cowley, S., Provan, G., ... others (2011). Periodic motion of saturn's nightside plasma sheet. *Journal of Geophysical Research: Space Physics*, *116*(A11). doi: 10.1029/2011JA016827

Arridge, C., Khurana, K., Russell, C., Southwood, D., Achilleos, N., Dougherty, M., ... Leinweber, H. (2008). Warping of saturn's magnetospheric and magnetotail current sheets. *Journal of Geophysical Research: Space Physics*, *113*(A8). doi: 10.1029/2007JA012963

Arridge, C., Russell, C., Khurana, K., Achilleos, N., Cowley, S., Dougherty, M., ... Bunce, E. (2008). Saturn's magnetodisc current sheet. *Journal of Geophysical Research: Space Physics*, *113*(A4). doi: 10.1029/2007JA012540

Bertucci, C., Achilleos, N., Dougherty, M., Modolo, R., Coates, A., Szego, K., ... others (2008). The magnetic memory of titan's ionized atmosphere. *Science*, *321*(5895), 1475–1478. doi: 10.1126/science.1159780

Bertucci, C., Hamilton, D., Kurth, W., Hospodarsky, G., Mitchell, D., Sergis, N., ... Dougherty, M. (2015). Titan's interaction with the supersonic solar wind. *Geophysical Research Letters*, *42*(2), 193–200. doi: 10.1002/2014GL062106

Briggs, J., Brain, D., Cartwright, M., Eastwood, J., & Halekas, J. (2011). A statistical study of flux ropes in the martian magnetosphere. *Planetary and Space Science*, *59*(13), 1498–1505. doi: 10.1016/j.pss.2011.06.010

Burlaga, L. (1988). Magnetic clouds and force-free fields with constant alpha. *Journal of Geophysical Research: Space Physics*, *93*(A7), 7217–7224. doi: 10.1029/JA093iA07p07217

Burlaga, L., Klein, L., Sheeley Jr, N., Michels, D., Howard, R., Koomen, M., ... Rosenbauer, H. (1982). A magnetic cloud and a coronal mass ejection. *Geophysical Research Letters*, *9*(12), 1317–1320. doi: 10.1029/GL009i012p01317

Chen, P., & Shibata, K. (2000). An emerging flux trigger mechanism for coronal mass ejections. *The Astrophysical Journal*, *545*(1), 524. doi: 10.1086/317803

Cravens, T., Robertson, I., Clark, J., Wahlund, J.-E., Waite Jr, J., Ledvina, S., ... others (2005). Titan's ionosphere: Model comparisons with cassini ta data. *Geophysical Research Letters*, *32*(12). doi: 10.1029/2005GL023249

DiBraccio, G. A., Slavin, J. A., Imber, S. M., Gershman, D. J., Raines, J. M., Jackman, C. M., ... others (2015). Messenger observations of flux ropes in mercurys magnetotail. *Planetary and Space Science*, *115*, 77–89. doi: 10.1016/j.pss.2014.12.016

Dougherty, M., Kellock, S., Southwood, D., Balogh, A., Smith, E., Tsurutani, B., ... others (2004). The cassini magnetic field investigation. In *The cassini-huygens mission* (pp. 331–383). Springer. doi: 10.1007/s11214-004-1432-2

Edberg, N., Wahlund, J.-E., Ågren, K., Morooka, M. W., Modolo, R., Bertucci, C., & Dougherty, M. (2010). Electron density and temperature measurements in the cold plasma environment of titan: Implications for atmospheric escape. *Geophysical Research Letters*, *37*(20). doi: 10.1029/2010GL044544

Elphic, R., Luhmann, J., Russell, C., & Brace, L. (1981). Magnetic flux ropes in the venus ionosphere: In situ observations of force-free structures? *Advances in Space Research*, *1*(9), 53–58. doi: 10.1016/0273-1177(81)90218-0

Elphic, R., & Russell, C. (1983a). Global characteristics of magnetic flux ropes in the venus ionosphere. *Journal of Geophysical Research: Space Physics*, *88*(A4), 2993–3003. doi: 10.1029/JA088iA04p02993

Elphic, R., & Russell, C. (1983b). Magnetic flux ropes in the venus ionosphere:

Observations and models. *Journal of Geophysical Research: Space Physics*, *88*(A1), 58–72. doi: 10.1029/JA088iA01p00058

Feyerabend, M., Simon, S., Neubauer, F. M., Motschmann, U., Bertucci, C., Edberg, N. J., ... Kurth, W. S. (2016). Hybrid simulation of titan's interaction with the supersonic solar wind during cassini's t96 flyby. *Geophysical Research Letters*, *43*(1), 35–42. doi: 10.1002/2015GL066848

Hidalgo, M., Cid, C., Vinas, A., & Sequeiros, J. (2002). A non-force-free approach to the topology of magnetic clouds in the solar wind. *Journal of Geophysical Research: Space Physics*, *107*(A1), SSH1–1. doi: 10.1029/JA088iA04p02993

Kabanovic, S., Simon, S., Neubauer, F. M., & Meeks, Z. (2017). An empirical model of titan's magnetic environment during the cassini era: Evidence for seasonal variability. *Journal of Geophysical Research: Space Physics*, *122*(11), 11–076. doi: 10.1002/2017JA024402

Keller, C., Cravens, T., & Gan, L. (1992). A model of the ionosphere of titan. *Journal of Geophysical Research: Space Physics*, *97*(A8), 12117–12135. doi: 10.1029/92JA00231

Kleeorin, N., Rogachevskii, I., & Eviatar, A. (1994). A mechanism of magnetic flux rope formation in the ionosphere of venus. *Journal of Geophysical Research: Space Physics*, *99*(A4), 6475–6481. doi: 10.1029/92JA00231

Ledvina, S., Nunes, D., Cravens, T., & L. Tinker, J. (2002). Pressure balance across magnetic flux ropes in the ionosphere of venus. *Journal of Geophysical Research: Space Physics*, *107*(A6), SMP–7. doi: 10.1029/2001JA900147

Lepping, R., Berdichevsky, D., & Wu, C.-C. (2017). Average magnetic field magnitude profiles of wind magnetic clouds as a function of closest approach to the clouds axes and comparison to model. *Solar Physics*, *292*(2), 27. doi: 10.1007/s11207-016-1040-9

Luhmann, J., & Elphic, R. (1985). On the dynamo generation of flux ropes in the venus ionosphere. *Journal of Geophysical Research: Space Physics*, *90*(A12), 12047-12056. doi: 10.1029/JA090iA12p12047

Martin, C., & Arridge, C. S. (2017). Cassini observations of aperiodic waves on saturn's magnetodisc. *Journal of Geophysical Research: Space Physics*, *122*(8), 8063–8077. doi: 10.1002/2017JA024293

Martin, C., & Arridge, C. S. (2019). Current density in saturn's equatorial current sheet: Cassini magnetometer observations. *Journal of Geophysical Research: Space Physics*, *124*(1), 279–292. doi: 10.1029/2018JA025970

Martin, C., Arridge, C. S., Badman, S. V., Billett, D. D., & Barratt, C. J. (Submitted). Modeling flux ropes in titan's ionosphere.

Mouschovias, T. C., & Poland, A. (1978). Expansion and broadening of coronal loop transients-a theoretical explanation. *The Astrophysical Journal*, *220*, 675–682. doi: 10.1086/155951

Ness, N., Acuna, M. H., Behannon, K. W., & Neubauer, F. M. (1982). The induced magnetosphere of titan. *Journal of Geophysical Research: Space Physics*, *87*(A3), 1369–1381. doi: 10.1029/JA087iA03p01369

Neubauer, F., Backes, H., Dougherty, M., Wennmacher, A., Russell, C., Coates, A., ... others (2006). Titan's near magnetotail from magnetic field and electron plasma observations and modeling: Cassini flybys ta, tb, and t3. *Journal of Geophysical Research: Space Physics*, *111*(A10). doi: 10.1029/2006JA011676

Omidi, N., Sulaiman, A. H., Kurth, W., Madanian, H., Cravens, T., Sergis, N., ... Edberg, N. J. (2017). A single deformed bow shock for titan-saturn system. *Journal of Geophysical Research: Space Physics*, *122*(11), 11–058. doi: 10.1002/2017JA024672

Osherovich, V., Farrugia, C., & Burlaga, L. (1995). Nonlinear evolution of magnetic flux ropes: 2. finite beta plasma. *Journal of Geophysical Research: Space Physics*, *100*(A7), 12307–12318. doi: 10.1029/95JA00273

Pilkington, N., Achilleos, N., Arridge, C. S., Guio, P., Masters, A., Ray, L., ...

Dougherty, M. (2015). Internally driven large-scale changes in the size of saturn's magnetosphere. *Journal of Geophysical Research: Space Physics*, *120*(9), 7289–7306. doi: 10.1002/2015JA021290

Provan, G., Andrews, D. J., Arridge, C. S., Coates, A. J., Cowley, S., Cox, G., ... Jackman, C. (2012). Dual periodicities in planetary-period magnetic field oscillations in saturn's tail. *Journal of Geophysical Research: Space Physics*, *117*(A1). doi: 10.1029/2011JA017104

Russell, C. (1990). Magnetic flux ropes in the ionosphere of venus. *Physics of Magnetic Flux Ropes*, *58*, 413–423. doi: 10.1029/GM058p0413

Russell, C., Berchem, J., & Luhmann, J. G. (1985). On the source region of flux transfer events. *Advances in space research*, *5*(4), 363-368. doi: 10.1016/0273-1177(85)90162-0

Russell, C., & Elphic, R. (1979). Observation of magnetic flux ropes in the venus ionosphere. *Nature*, *279*(5714), 616. doi: 10.1038/279616a0

Simon, S., van Treeck, S. C., Wennmacher, A., Saur, J., Neubauer, F. M., Bertucci, C. L., & Dougherty, M. K. (2013). Structure of titan's induced magnetosphere under varying background magnetic field conditions: Survey of cassini magnetometer data from flybys ta–t85. *Journal of Geophysical Research: Space Physics*, *118*(4), 1679–1699. doi: 10.1002/jgra.50096

Simon, S., Wennmacher, A., Neubauer, F. M., Bertucci, C. L., Kriegel, H., Saur, J., ... Dougherty, M. K. (2010). Titan's highly dynamic magnetic environment: A systematic survey of cassini magnetometer observations from flybys ta–t62. *Planetary and Space Science*, *58*(10), 1230–1251. doi: 10.1016/j.pss.2010.04.021

Slavin, J., Lepping, R., Gjerloev, J., Fairfield, D., Hesse, M., Owen, C., ... Mukai, T. (2003). Geotail observations of magnetic flux ropes in the plasma sheet. *Journal of Geophysical Research: Space Physics*, *108*(A1), SMP–10. doi: 10.1029/2002JA009557

Slavin, J., Lepping, R. P., Wu, C.-C., Anderson, B. J., Baker, D. N., Benna, M., ... others (2010). Messenger observations of large flux transfer events at mercury. *Geophysical Research Letters*, *37*(2). doi: 10.1029/2009GL041485

Smith, A., Jackman, C., & Thomsen, M. (2016). Magnetic reconnection in saturn's magnetotail: A comprehensive magnetic field survey. *Journal of Geophysical Research: Space Physics*, *121*(4), 2984–3005. doi: 10.1002/2015JA022005

Smith, A., Jackman, C., Thomsen, M., Sergis, N., Mitchell, D., & Roussos, E. (2018). Dipolarization fronts with associated energized electrons in saturn's magnetotail. *Journal of Geophysical Research: Space Physics*, *123*(4), 2714–2735. doi: 10.1002/2017JA024904

Smith, A., Slavin, J., Jackman, C., Poh, G.-K., & Fear, R. (2017). Flux ropes in the hermean magnetotail: Distribution, properties, and formation. *Journal of Geophysical Research: Space Physics*, *122*(8), 8136–8153. doi: 10.1002/2017JA024295

Sonnerup, B. Ö., & Cahill Jr, L. (1967). Magnetopause structure and attitude from explorer 12 observations. *Journal of Geophysical Research*, *72*(1), 171–183. doi: 10.1029/JZ072i001p00171

Thomsen, M., Wilson, R., Tokar, R., Reisenfeld, D., & Jackman, C. M. (2013). Cassini/caps observations of duskside tail dynamics at saturn. *Journal of Geophysical Research: Space Physics*, *118*(9), 5767–5781. doi: 10.1002/jgra.50552

Vasyliunas, V. M. (1983). Plasma distribution and flow. *Physics of the Jovian magnetosphere*, 395–453.

Vignes, D., Acuña, M., Connerney, J., Crider, D., Rème, H., & Mazelle, C. (2004). Magnetic flux ropes in the martian atmosphere: Global characteristics. In *Mars magnetism and its interaction with the solar wind* (pp. 223–231). Springer. doi: 10.1023/B:SPAC.0000032716.21619.f2

Wei, H., Russell, C., Dougherty, M., Ma, Y., Hansen, K., McAndrews, H., ...

Young, D. (2011). Unusually strong magnetic fields in titans ionosphere: T42 case study. *Advances in Space Research*, *48*(2), 314–322. doi: 10.1016/j.asr.2011.02.009

Wei, H., Russell, C., Dougherty, M., Neubauer, F., & Ma, Y. (2010). Upper limits on titan's magnetic moment and implications for its interior. *Journal of Geophysical Research: Planets*, *115*(E10). doi: 10.1029/2009JE003538

Wei, H., Russell, C., Zhang, T., & Dougherty, M. (2010). Comparison study of magnetic flux ropes in the ionospheres of venus, mars and titan. *Icarus*, *206*(1), 174–181. doi: 10.1016/j.icarus.2009.03.014

Wolff, R., Goldstein, B., & Yeates, C. (1980). The onset and development of kelvin-helmholtz instability at the venus ionopause. *Journal of Geophysical Research: Space Physics*, *85*(A13), 7697–7707. doi: 10.1029/JA085iA13p07697

Yelle, R. V., Borggren, N., De La Haye, V., Kasprzak, W., Niemann, H., Müller-Wodarg, I., & Waite Jr, J. (2006). The vertical structure of titan's upper atmosphere from cassini ion neutral mass spectrometer measurements. *Icarus*, *182*(2), 567–576. doi: 10.1016/j.icarus.2005.10.029

Zhang, T., Baumjohann, W., Teh, W., Nakamura, R., Russell, C., Luhmann, J., ... others (2012). Giant flux ropes observed in the magnetized ionosphere at venus. *Geophysical Research Letters*, *39*(23). doi: 10.1029/2012GL054236

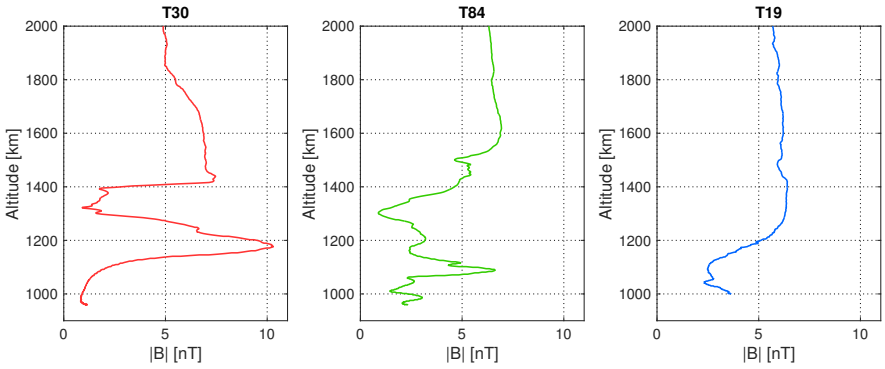

Figure 1. Figure showing three examples of altitude profiles of magnetic field magnitude. Red: T30 with a large flux rope at 1150 km when Titan is at 13.6 SLT. Green: T84 flyby with flux rope at 1100 km when Titan is at 13.7 SLT. Both of these profiles are taken from times when Titan is in the magnetosheath or current sheet according to the classification scheme from (Simon et al., 2010, 2013). Blue: T19, an example with no flux ropes when Titan is at 2.2 SLT and primarily in the southern lobe of Saturn according to (Simon et al., 2010).

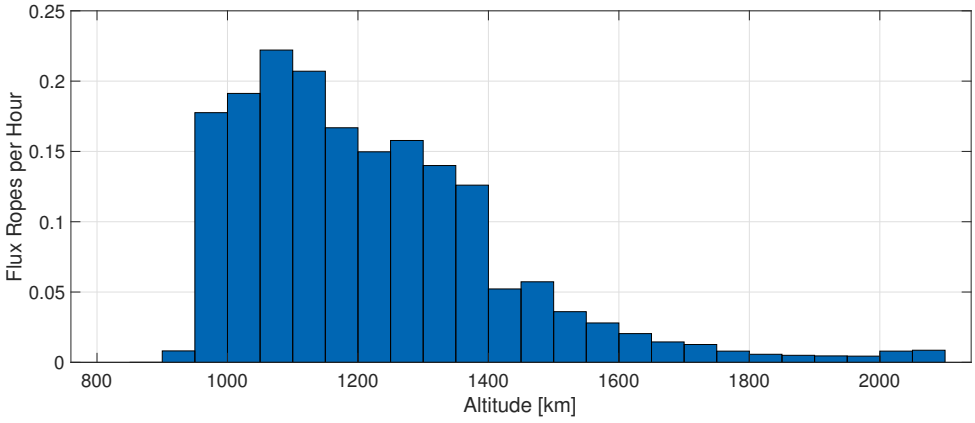

Figure 2. Figure showing the altitude distribution of flux ropes in Titan's ionosphere normalised by the number of hours that Cassini spent within the altitude bin for all flybys.

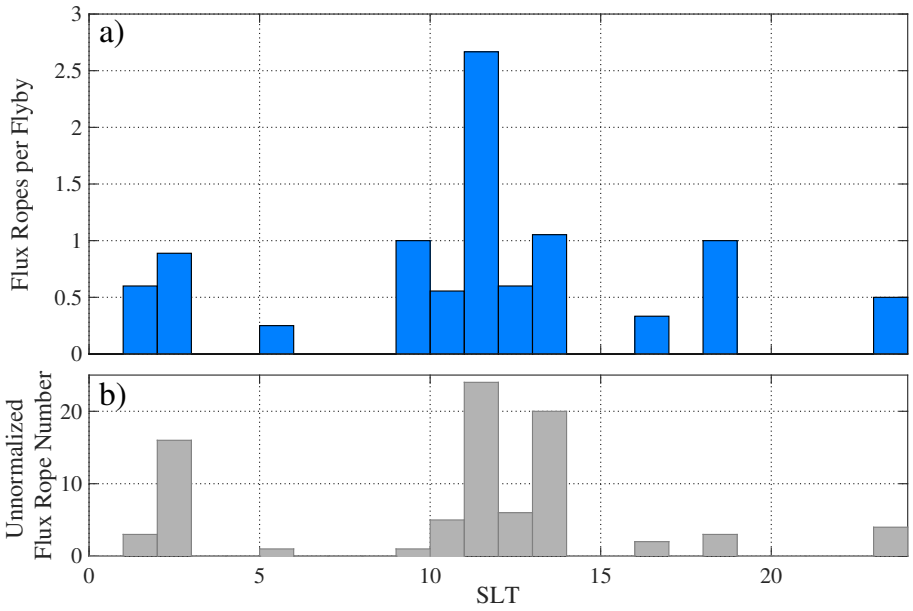

Figure 3. Figure showing the Saturn local time distribution of flux ropes in Titan's ionosphere, a) normalized by number of flybys in each SLT sector and b) unnormalized.

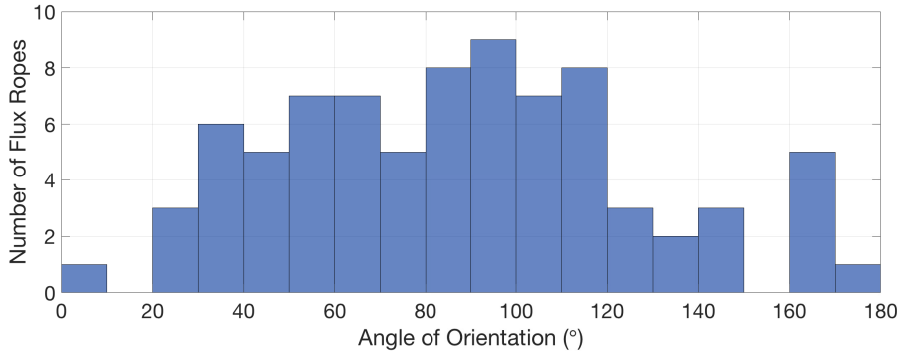

Figure 4. Figure showing the orientation of flux ropes at Titan with respect to the surface of Titan.

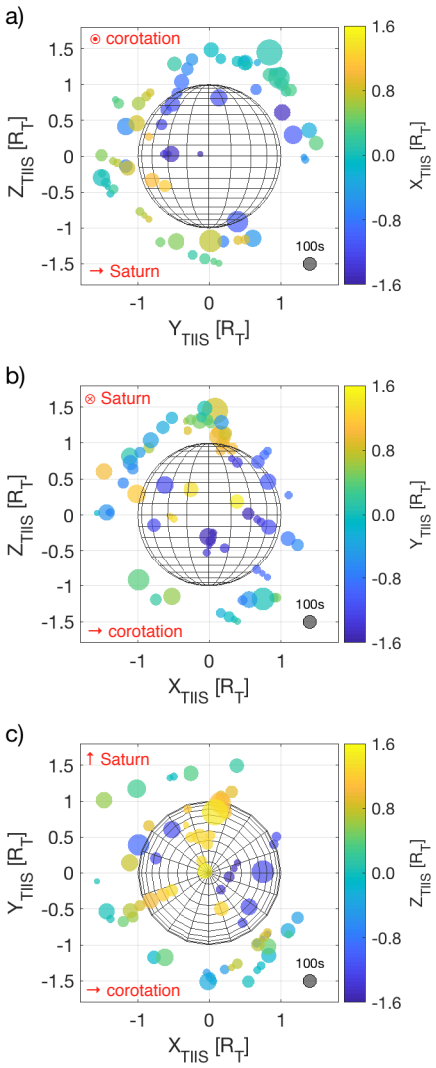

Figure 5. Figure showing the position of flux ropes at Titan in the TIIS coordinate system. The size of each point is determined by the length of time that Cassini was detecting the flux rope, where 100 seconds is shown by the key. Titan's outline is shown in black and each flux rope is a coloured circle, coloured by position in the third dimension.

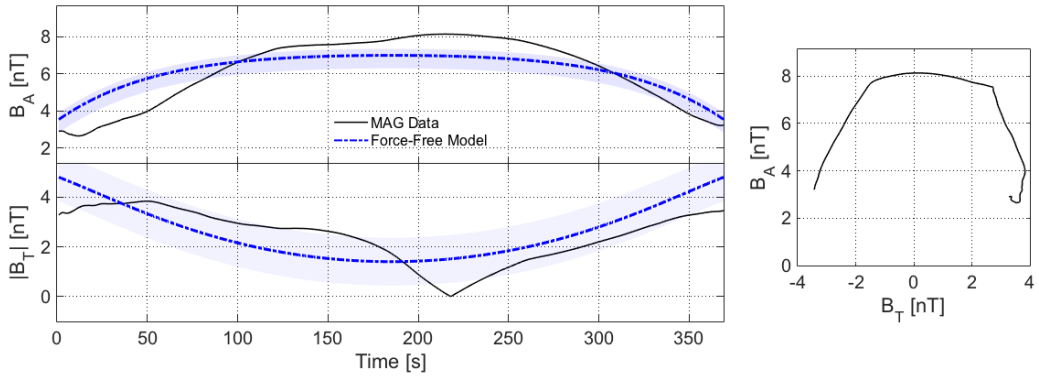

Figure 6. Figure showing an example of a flux rope signature in magnetometer data (black) fitted with a force-free model (blue) with uncertainty range (pale blue range). The figure shows axial magnetic field and tangential magnetic field. On the right is a hodogram showing the relationship between the axial and tangential field components. This flux rope occurred at 5.3 SLT on 16th April 2005 at 19:05 during flyby T5.

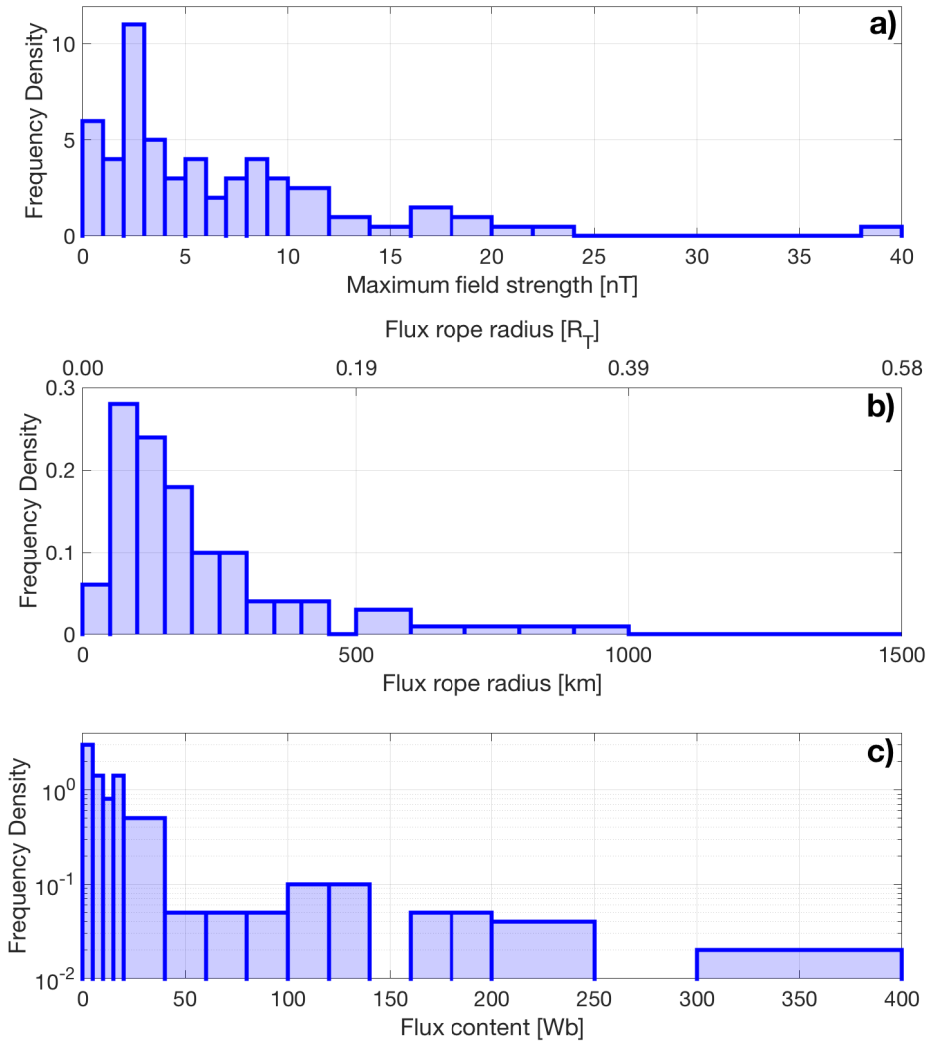

Figure 7. Figure showing a histogram of a) maximum core magnetic field, b) flux rope radius and c) flux content for 49 flux rope in Titan's ionosphere that fit to the force-free model with an MSE of 0.5 or below and P(χ^2) of 5% or less.

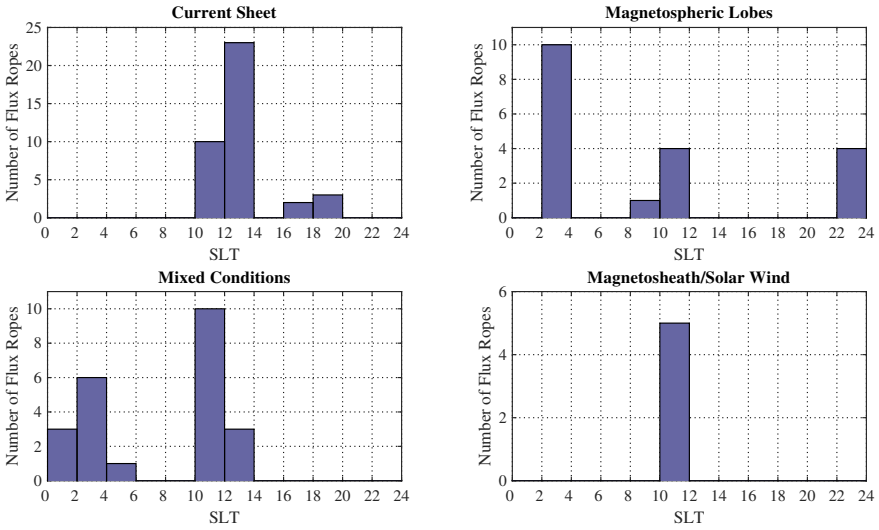

Figure 8. Histogram of the number of flux ropes with SLT ordered by magnetic environment which is determined by (Simon et al., 2010, 2013; Kabanovic et al., 2017).

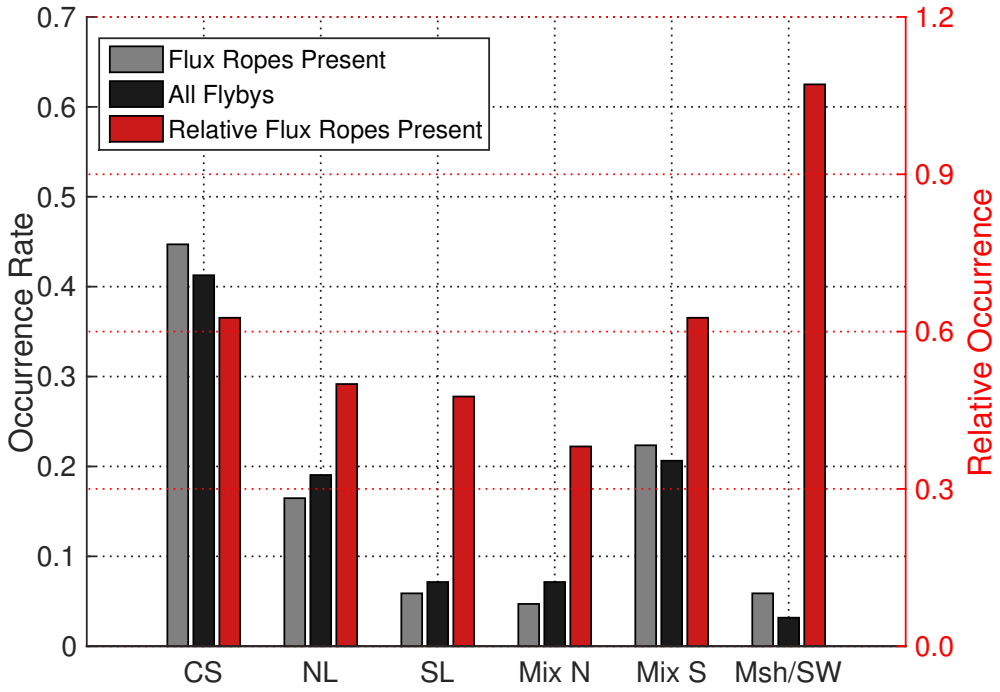

Figure 9. Histogram of the occurrence rate of different magnetospheric environments at ±3 hours of all flybys of Titan (black, black axis), all flybys with flux ropes present (grey, black axis), and a relative occurrence of each environment where flux ropes are present relative to the occurrence rate of all flybys (red, red axis). Where CS is the current sheet, NL is the northern lobe, SL is the southern lobe, Mix N/S are a mixture with primarily northern (N) or southern (S) signatures and Msh/SW is magnetosheath or solar wind. Magnetic environment is determined by (Simon et al., 2010, 2013; Kabanovic et al., 2017).

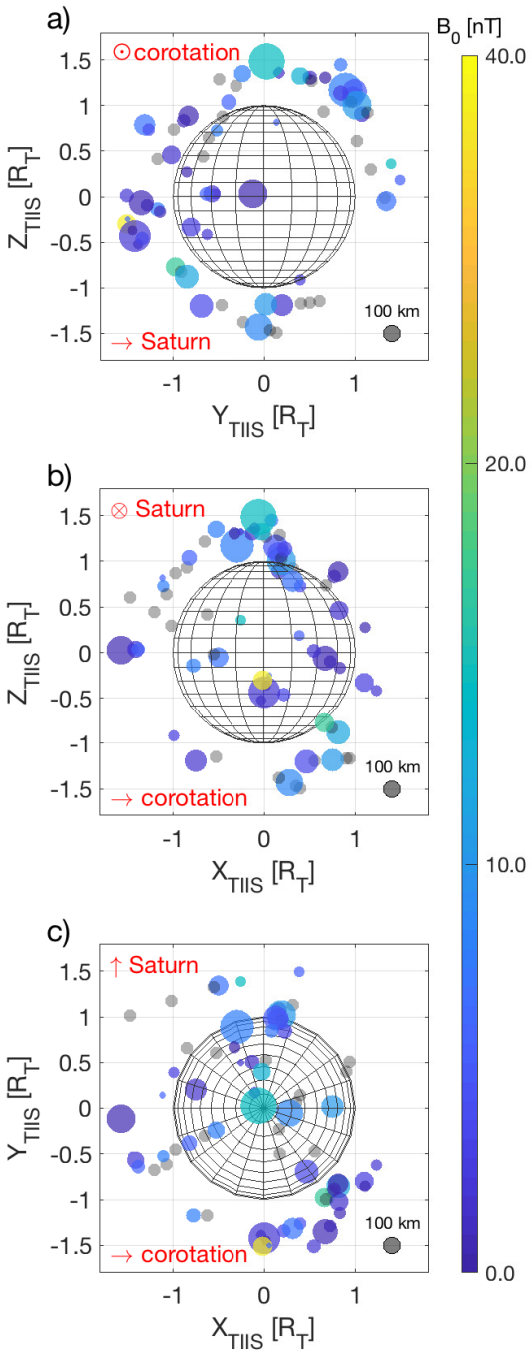

Figure 10. Figure showing the position of flux ropes at Titan in the TIIS coordinate system. The size of each point is determined by the radius found using the force-free models, where a 100 km example is shown by the key. Titan's outline is shown in black and each flux rope is a coloured circle, coloured by magnetic field strength in the centre of the flux rope. Flux ropes which were not fitted by the force-free model are shown in grey with a 100 km equivalent radius.